PCCP

Accepted Manuscript

This is an *Accepted Manuscript*, which has been through the Royal Society of Chemistry peer review process and has been accepted for publication.

Accepted Manuscripts are published online shortly after acceptance, before technical editing, formatting and proof reading. Using this free service, authors can make their results available to the community, in citable form, before we publish the edited article. We will replace this *Accepted Manuscript* with the edited and formatted *Advance Article* as soon as it is available.

You can find more information about *Accepted Manuscripts* in the **Information for Authors**.

Please note that technical editing may introduce minor changes to the text and/or graphics, which may alter content. The journal's standard **Terms & Conditions** and the **Ethical guidelines** still apply. In no event shall the Royal Society of Chemistry be held responsible for any errors or omissions in this *Accepted Manuscript* or any consequences arising from the use of any information it contains.

Theoretical studies of molecular orientation and charge recombination in poly-*para*phenylenevinylene light-emitting diodes

Koharu Aikawa,[a] Masato Sumita,[b] Yasuyo Shimodo[c] and Kenji Morihashi*[a]

_____

*To whom correspondence should be addressed. E-mail: morihasi@chem.tsukuba.ac.jp

a) *Department of Chemistry, Graduate School of Pure and Applied Sciences, University of Tsukuba, 1-1-1, Tennodai, Tsukuba, Ibaraki 305-8571, Japan*

b) *National Institute for Materials Science (NIMS), 1-1 Namiki, Tsukuba, Ibaraki 305-0044, Japan*

c) *Faculty of Pharmacy, Yasuda Women's University, 6-13-1 Yasuhigashi, Asaminami-ku, Hiroshima 731-0153, Japan*

Abstract

Poly-*para*phenylenevinylene (PPV), a material used in organic light-emitting diodes (OLEDs), for which improving the efficiency is an important issue. In general, the molecular orientations of organic compounds in crystal form are an essential factor determining electron and hole transfer, which are closely related to the efficiency of OLEDs. We have investigated the effects of the rotation of each molecule and the intermolecular distance in the dimer system of PPV, which consists of donor and acceptor molecules, on its charge-recombination process by performing constrained density functional calculations. Starting from the structure of the crystal, it was clarified that the rotation of the donor decreases the charge-recombination factor, to nearly zero, while that of the acceptor increases it to about 10^6 s^{-1}. We found that this is caused by the repulsive interaction between the donor and acceptor molecules and the formation of a transport pathway resulting from the acceptor rotation.

Keywords: Organic light-emitting diode (OLED); Charge recombination; Constrained density functional theory (CDFT); Marcus parameters; Driving force.

1.   Introduction

Organic semiconductors, which are used in organic light-emitting diodes (OLEDs),

organic field-effect transistors (OFETs), and organic solar cells, are attracting

considerable interest because of their charge-transport properties. The performance of

organic semiconductors has been increased to that of inorganic semiconductors such as

silicon in recent studies.[1–5] In most of these studies, great effort has been made to

promote charge mobility, which is an important factor when evaluating the performance

of organic semiconductors.[6–9]

   The emissive electroluminescence layer of OLEDs is a film of an organic

semiconductor. OLEDs often use a thin polymer film fabricated by vacuum

evaporation/sublimation or solution-casting or printing technologies. In the case of

solution-casting technology, the performance of the OLEDs is strongly affected by the

type of solution. For example, a poly-*para*phenylenevinylene (PPV)-based polymer

film with a chlorobenzene solvent exhibits larger field-effect hole mobility than one

with toluene. This difference in the hole mobility is attributed to the difference in the

molecular alignment in the film.[10,11]

Generally, π-conjugated molecules such as PPV often aggregate in a π-stacked form.[12,13] These π-stacked structures have a large transfer integral; this parameter represents the probability of adiabatic electron transfer (ET) in the conjugated material.[2,6,8,14] On the other hand, the mobilities in the crystalline derivative of tetrathiafulvalene increase in the order of partial stacking, lamella (stacking), and the herringbone structure.[15] Similarly, the herringbone structures of rubrene and tetracene exhibit very high mobilities of 24.5 and 5 cm^2/Vs, respectively.[3,6,16,17] According to previous studies, these high mobilities in the herringbone structure are due to the small grain-boundary effect[1] and the smaller electrostatic repulsion in the herringbone structure[2] than that in the π-stacked structure. This indicates that the transfer integral alone is insufficient to discuss the ET reaction. We focus on not only the transfer integral but also the other parameters in Marcus theory: the driving force $-\Delta G^{\circ}$ and the reorganization energy λ. As explained in section 2.2, because these parameters are inside the exponential in the equation for the ET rate constant, changes in these values induce a large change in the rate constant.
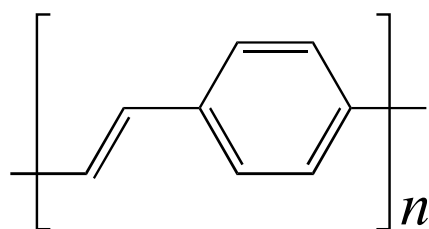
SCHEME 1   **PPV**

PPV is used in OFETs such as OLEDs and in organic solar cells using the opposite

reaction to that in OLEDs.[4] PPV has thus attracted considerable attention as an OELD

material.[18] The working principle of the luminescence process of PPV as an OLED

material is based on charge injection as shown in Fig. 1; first, electrons and holes are

injected from the electrodes to the PPV layer, and the collision between holes and

electrons with charge recombination induces an ET reaction. Then the holes and

electrons form excited acceptor molecules, and the PPV emits light when it returns to
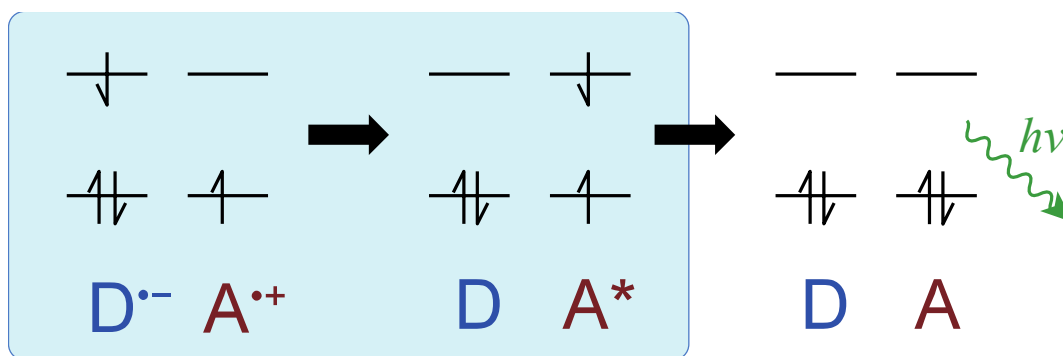
the ground state.

Fig. 1   Luminescence process based on charge injection. The blue shaded area shows the

charge recombination process focused on in this study. D and A represent the donor and

acceptor molecules, respectively. In this study, we concentrate the triplet-triplet charge recombination process.

The maximum ratio of the quantum efficiencies for electroluminescence and photoluminescence (QE(EL)/QE(PL)) is theoretically 25% because of the generation ratio of the singlet to the triplet. However, Cao *et al.*[19] have measured the efficiency of PPV-based OLEDs to be as high as ~50% in experiments. To clarify the origin of such a high efficiency, Shuai *et al.*[20] investigated the behavior of excitons within the π☐electron approximation. According to their results, a high efficiency is achieved in the coherent electronic state, i.e., strong coupling. However, their study did not consider the structural dependence, that is, they computed only a cofacial arrangement in which PPV molecules were separated by 4.0 Å in their model of the bulk structure of PPV.

In this paper, we provide new perspectives that are different from those in previous studies concerning the use of PPV as an organic semiconductor in the following two points. First, previous studies discussed hole and/or electron transfer but not the charge recombination process. Second, these studies included the orientations applied for the model system of PPV treat only shifted on face-to-face orientation or yawing on Euler

angle,[2,14,20-22] even though the crystal structure of PPV has a rolled or pitched structure[23]

and a similar structure can appear in a thin film of PPV. The crystal structure of PPV has

herringbone packing.[23] The setting angle in the structure has been estimated to be

between 56 and 68˚. If PPV forms a thin film, its morphology will be amorphous.

According to a previous experimental study, the structure is the cylindrical with a local

stack structure, and its horizontal cross section has the edge-to-face form.[24] In this study,

we focus on the charge-recombination process, which is the final state before the

luminescence process, and the molecular alignments in the case of cofacial π-stacks and

roll displacements.

We calculate the charge recombination factor (which is likely to be the transfer rate

constant) and the Marcus parameters for the charge-recombination process of PPV

using constrained density functional theory (CDFT).[25–29] Although the

charge-recombination factor of the cofacial orientation in our study is very small (on the

order of 10^{-18}), several rotations result in a large recombination factor of up to $\sim 10^8$.

Further, we show that the angle of rotation is considerably different for the donor and

acceptor molecules.

2. Models and methods

2.1 Model systems
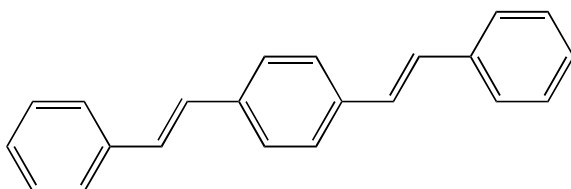
SCHEME 2   **OPV3**

Because PPV polymers are too large for CDFT calculations, we used

oligo-*para*phenylene vinylene, which contains three phenyl rings (OPV3), as the model

system for PPV. The dimer system consists of two molecules, donor and acceptor

molecules. The initial state (i.e., the polaron pair) of the OPV3 dimer is the complex of

the radical anion ($^2D^{\bullet-}$) and radical cation ($^2A^{\bullet+}$) states of OPV3, which we represent as

$\{^2D^{\bullet-}...^2A^{\bullet+}\}$. The final state (i.e., the exciton pair) of the OPV3 dimer is the complex of

the ground (^1D) and excited triplet ($^3A^*$) states, which we represent as $\{^1D...^3A^*\}$. The

monomer structures generating dimer pairs, $^2D^{\bullet-}$, $^2A^{\bullet+}$, ^1D, and $^3A^*$, are optimized,

respectively and arranged as the dimer system.

The molecular center-to-center distance in the face-to-face dimer is set to 4.0 Å,

similarly to in previous studies.[14,20,21] Upon rotational orientation, the donor or acceptor

of the dimer is rotated around the principal axis of inertia (the x-axis in Fig. 2). We refer

to this as *roll* rotation by the Euler angle.

In tilted orientations, the default site-site distance was set to 2.9 Å for the closest

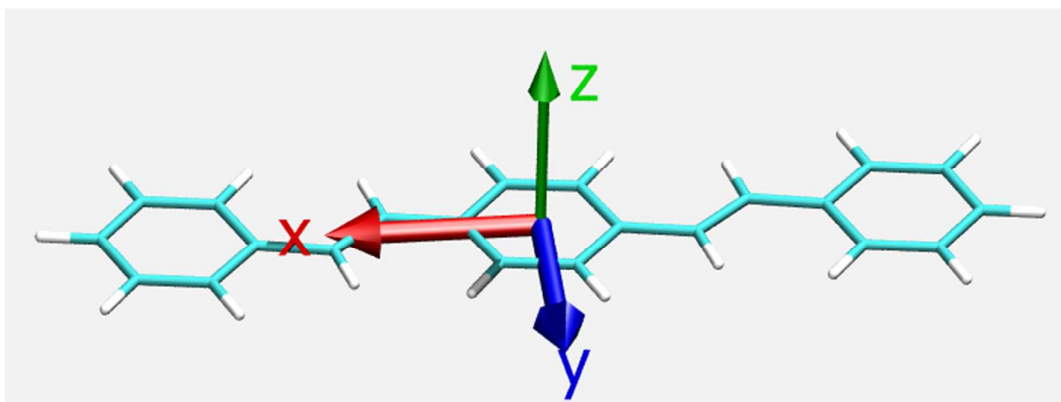hydrogen-hydrogen distance between the tilted and planar sites (Fig. 3).

Fig. 2   **Principal inertia axes x, y, and z, of OPV3. In this study, the x-, y-, and z-axis**

rotations of the molecular frame are referred to roll, pitch, and yaw rotations, respectively.
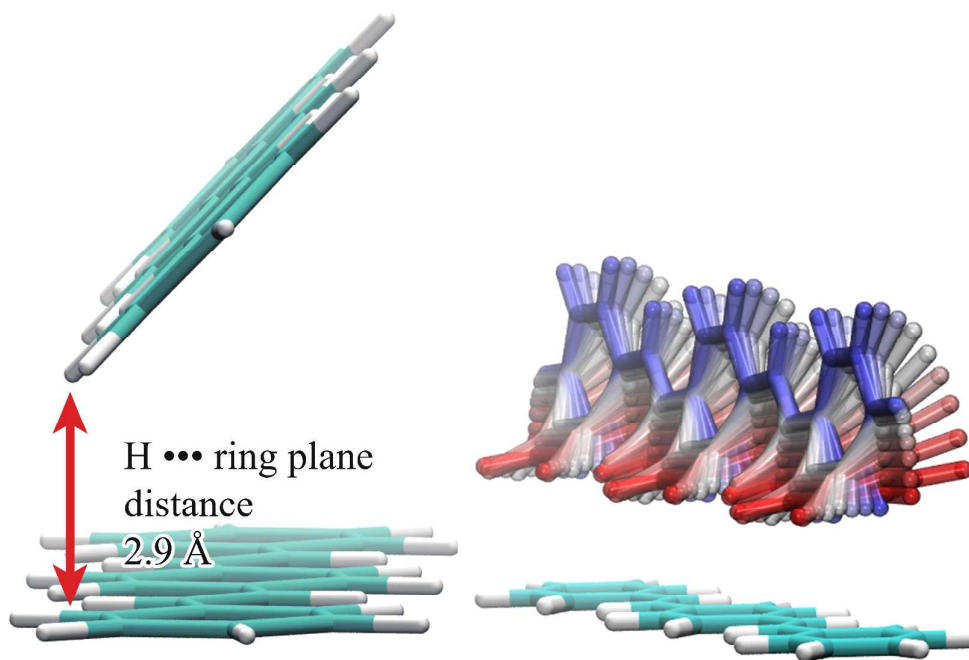
Fig. 3 **Closest-contact distance when the upper molecule is tilted (left) and rotated from 10° to 90° (right).**

In the investigation of the possible form of the dimer in the charge-recombination process of OPV3, the charge transfer properties of the crystal form will provide information on the likely OPV3-dimer system. However, we have no data for the OPV3 crystal. As an alternative, to find the likely OPV3-dimer form, we investigate the methyl-substituted OPV3 (OPV3-methyl, Scheme 3) system, because the single-crystal structure has been determined by X-ray analysis.[30] Thus, the geometric alignment of the OPV3-methyl dimer that minimizes the root-mean-square deviation for the crystal

structure was calculated using PyMOL.
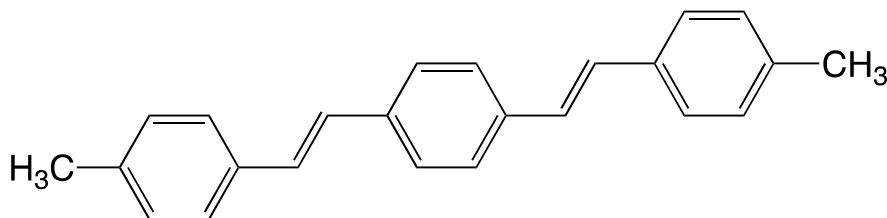
SCHEME 3   **OPV3-methyl**

2.2   Charge-recombination process calculations

We focus on the charge recombination factor k and its parameters in the Marcus-Hush

equation, i.e., the reorganization energy λ, the driving force $-\Delta G^\circ$, and the transfer

integral H_{ab}. Using Marcus theory,[31] we predict k and the parameters of the four states,

which can be represented as combinations of the electronic and molecular structures of

the initial and final states as shown in Fig. 4 and Table 1. The driving force $-\Delta G^\circ$ and

reorganization energy λ are estimated from the differences between the energies of the

four points shown in Fig. 4, and the following equation gives the charge recombination

factor:

$$k = \frac{2\pi}{\hbar} \frac{1}{\sqrt{4\pi\lambda k_\mathrm{B} T}} H_{ab}^2 \exp\left(-\frac{(\Delta G^\circ + \lambda)^2}{4\lambda k_\mathrm{B} T}\right), \qquad (1)$$

where k_B is the Boltzmann constant and T is the temperature. The activation energy is

defined as

$$\Delta G^{\ddagger} = \frac{\left(\Delta G^{\circ} + \lambda\right)^2}{4\lambda} .$$
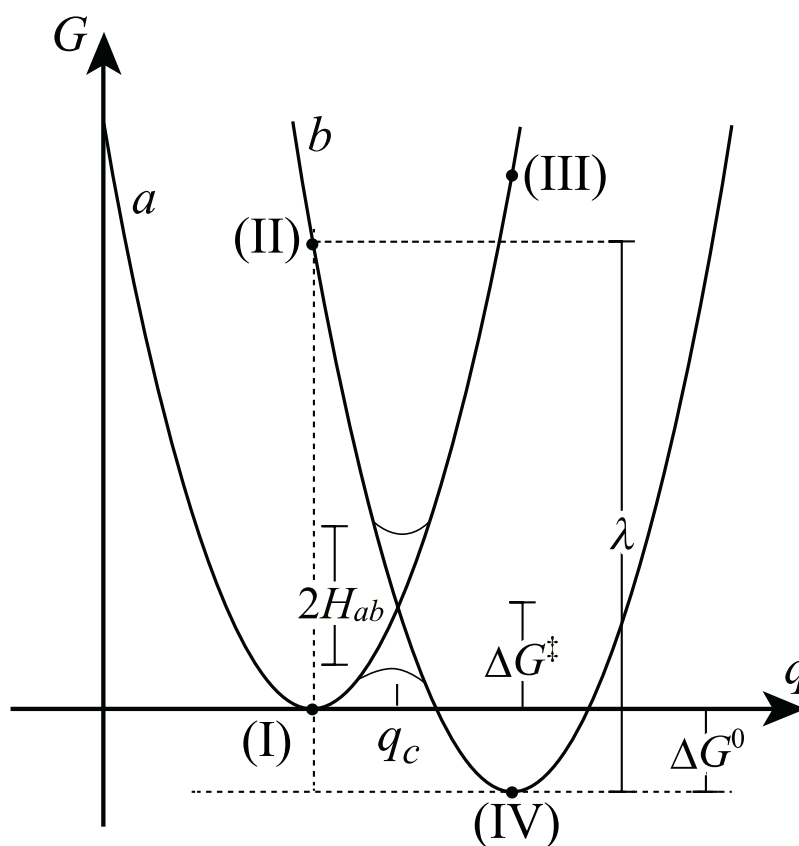

Fig. 4 **Schematic free-energy curves obtained by Marcus theory for ET process. Parabolas**

***a* and *b* are the initial and final electronic states, respectively. Points (I) and (II) represent the**

initial states in the ET reaction and points (III) and (IV) represent the final states.

Table 1 **Molecular and electronic structures at the four points in Fig. 4. $\{^2D^{\bullet-}-^2A^{\bullet+}\}$ and $\{^1D-^3A^*\}$ denote the initial and final states, respectively.**

System	Molec. Structure	Elec. Structure
(I)	$\{^2D^{\bullet-}-^2A^{\bullet+}\}$	$\{^2D^{\bullet-}-^2A^{\bullet+}\}$
(II)	$\{^2D^{\bullet-}-^2A^{\bullet+}\}$	$\{^1D-^3A^*\}$
(III)	$\{^1D-^3A^*\}$	$\{^2D^{\bullet-}-^2A^{\bullet+}\}$
(IV)	$\{^1D-^3A^*\}$	$\{^1D-^3A^*\}$

Note that we approximated the Gibbs free energy by the total energy of a single point

calculation in the calculation of $\Delta G°$. We should use the free energy to obtain the

quantitatively correct parameters, but this requires the computation of the external

field.[28] Fortunately, the qualitative trend is sufficient for the discussion in this work, and

therefore we ignored the change in entropy ΔS. This is valid because the structural

change between the initial and final states is small in the solid and amorphous states.[32]

13

2.3   Constrained DFT

In density functional theory (DFT), the delocalized electronic structure is erroneously

estimated to be more stable state than the charge-localized structure owing to the

self-interaction error.[33] For this reason, several methods have been developed to correct

this error: the self-interaction correction by Perdew and Zunger,[34] the DFT+U method

using the Hubbard U model,[35] the long-range correction scheme,[36] and the constrained

DFT[25-29] (CDFT) which imposes constraints on the charge or spin density of arbitrary

molecular fragments.

  In CDFT, the difference in the charge or spin density between fragments is

constrained. A general constraint on the density is described as

$$\sum_{\sigma} \int w_c^{\sigma}(\mathbf{r})\rho(\mathbf{r})\mathrm{d}\mathbf{r} = N_c,$$ (2)

where $w_c(\mathbf{r})$ is the weight function that defines the constrained property, ρ is the charge

density, σ represents the α or β spin, and N_c is the net difference in charge between the

donor and acceptor, i.e., $N_c = (N_D - N_A)/2$. The weight function is $w_c^{\alpha} = w_c^{\beta}$ for the

charge constraint on the system. On the other hand, the weight function $w_c^{\alpha} = -w_c^{\beta}$ for

the spin constraint.[37] The following energy functional, which is added to this constraint

14

term via a Lagrange multiplier V_c, is minimized during the SCF optimization.

$$W[\rho, V_c] = E[\rho] + V_c \left(\sum_\sigma \int w_c^\sigma(\mathbf{r})\rho(\mathbf{r})\,\mathrm{d}\mathbf{r} - N_c \right) \qquad (3)$$

Here, we demonstrate a typical example of the constraint term in CDFT when the region

C is constrained as shown in Fig.5. First, if the charge density is constrained, then

$$\left(\int_C \rho^\alpha(\mathbf{r})\,\mathrm{d}\mathbf{r} + \int_C \rho^\beta(\mathbf{r})\,\mathrm{d}\mathbf{r} \right) - \left(\int_{NC} \rho^\alpha(\mathbf{r})\,\mathrm{d}\mathbf{r} + \int_{NC} \rho^\beta(\mathbf{r})\,\mathrm{d}\mathbf{r} \right)$$
$$= \int_C \rho(\mathbf{r})\,\mathrm{d}\mathbf{r} - \int_{NC} \rho(\mathbf{r})\,\mathrm{d}\mathbf{r} = N_C - N_{NC} = N_c \qquad (4)$$

On the other hand, if the spin density is constrained, then

$$\left(\int_C \rho^\alpha(\mathbf{r})\,\mathrm{d}\mathbf{r} - \int_C \rho^\beta(\mathbf{r})\,\mathrm{d}\mathbf{r} \right) - \left(\int_{NC} \rho^\alpha(\mathbf{r})\,\mathrm{d}\mathbf{r} - \int_{NC} \rho^\beta(\mathbf{r})\,\mathrm{d}\mathbf{r} \right)$$
$$= \int_C \rho^s(\mathbf{r})\,\mathrm{d}\mathbf{r} - \int_{NC} \rho^s(\mathbf{r})\,\mathrm{d}\mathbf{r} = N_c, \qquad (5)$$
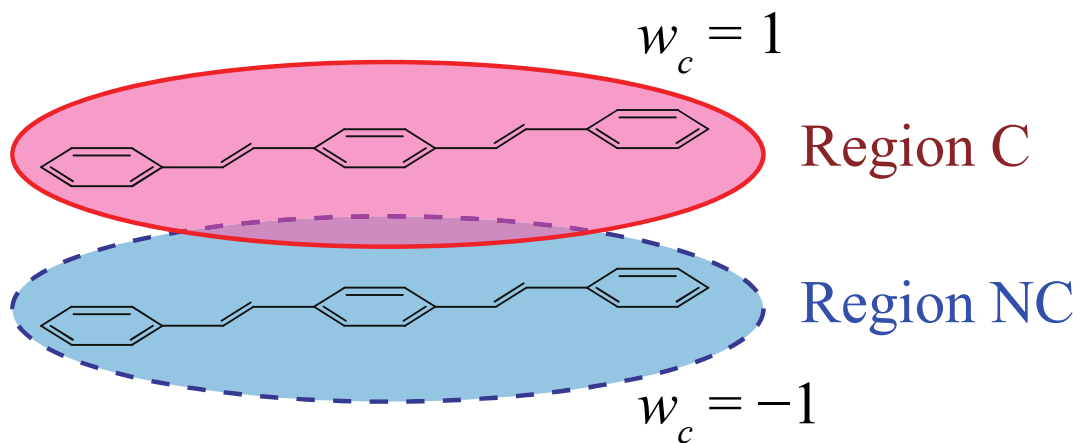
where ρ^s is the spin density.

Fig. 5　　**Region C is the constrained region, and Region NC is the nonconstrained region.**

Furthermore, Wu and Van Voorhis have developed CDFT method to calculate the

15

electronic coupling matrix element H_{ab}.[26] The following matrix **H** is obtained by using

$V_c w_c$ solved in the CDFT calculation:

$$\mathbf{H} = \begin{pmatrix} H_{DD} & H_{DA} \\ H_{AD} & H_{AA} \end{pmatrix},$$

where

$$
\begin{aligned}
H_{DD} &= \langle \Phi_D | H | \Phi_D \rangle = E[\rho_D] = E_D \\
H_{AA} &= E_A \\
H_{DA} &= \langle \Phi_D | H + V_c^A w_c - V_c^A w_c | \Phi_A \rangle \\
&= F_A \langle \Phi_D | \Phi_A \rangle - V_c^A \langle \Phi_D | w_c | \Phi_A \rangle \\
H_{AD} &= F_D \langle \Phi_A | \Phi_D \rangle - V_c^D \langle \Phi_A | w_c | \Phi_D \rangle
\end{aligned}
$$

and

$$F = \langle \Psi_c | H + V_c w_c | \Psi_c \rangle = E[\rho_c] + V_c \int w_c(\mathbf{r}) \rho(\mathbf{r}) \mathrm{d}\mathbf{r} = E + V_c N_c \ .$$

By orthogonalization between Φ_D and Φ_A, we can obtain the coupling matrix element

H_{ab} as the off-diagonal element.

3.　Computational details

Geometry optimization of the monomers was performed at the B3LYP/6-31G(d) level

with the Gaussian 09 package.[38] Dimer calculation by CDFT was performed using a

program developed in our laboratory[39] at the same level of theory. In all CDFT

16

calculations, we used the Becke weight population scheme to define the weight

functions. The electronic coupling matrix element H_{ab} was calculated using the

Kohn-Sham orbitals and the parameters V_c in the dimer calculations using our program.

In addition, we used the fragmented initial density matrix to improve the convergence

performance (details in Appendix).

4. Results and discussion

4.1 Face-to-face orientation and center-to-center distance

The calculations for OPV3 and OPV3-methyl were performed in the face-to-face

orientation (at a fixed center-to-center distance of 4.0 Å). Although the face-to-face

orientation has been used in many previous studies, the charge-recombination factor of

the orientation obtained in the present work using the CDFT calculation is very small

(10^{-18} s^{-1} order). These parameters and the charge recombination factor of OPV3 and

OPV3-methyl are shown in Table 2, and the relative energies of the four states (in Table

1 and Fig. 4) are shown in Table 3.

Table 2   Calculated charge recombination parameters[a] and decadic logarithm of charge recombination factor in the face-to-face orientation of the OPV3 and OPV3-methyl systems.

System	$-\Delta G°$	λ	$\Delta G^{\ddagger}$	$|H_{ab}|$	$\log_{10}(\kappa\,[\mathrm{s}^{-1}])$
FtoF OPV3	162.7	25.15	188.0	19.40	−17.80
FtoF OPV3-methyl	155.7	25.82	163.3	20.44	−13.45

[a] All energies are in kJ mol^{-1}.

Table 3   Calculated energies of four states [a] in **Fig.** 4 **in the face-to-face orientation of the OPV3 and OPV3-methyl systems.**

System	(I)	(II)	(III)	(IV)
FtoF OPV3	0.000	−137.5	25.43	−162.7
FtoF OPV3-methyl	0.000	−129.9	26.39	−155.7

[a] All energies are in kJ mol^{-1}.

When the center-to-center distance of OPV3 is increased, the recombination factor decreases as shown in Fig. 6. Figure 7 shows the energy variations of the four states with the center-to-center distance of the OPV3 dimer. The energy gaps between the initial states (I) and (III) and between the final states (II) and (IV) become larger as the distance increases. This indicates that PPV in the cofacial orientation has a large driving force in the case of a large intermolecular distance. Since the energies of the four states increases with decreasing center-to-center distance below 4.0 Å because of the van der Waals repulsion, as shown in Fig. 7, the center-to-center distance at which ET is

18

induced is estimated to be over 4.0 Å. In the face-to-face orientation, the recombination

factor is less than 1 s^{-1}, i.e., the value at 4.0 Å, which implies that the minimum

recombination factor of the polaron states, is only 10^{-18} s^{-1}.

The face-to-face orientation appears to be favorable for the charge recombination

reaction because of the large π-π overlap, but such a trend is not indicated by our results.

The reason why the face-to-face orientation is not favorable for charge recombination,

despite the feasible structure may be due to the large π-π electrostatic repulsion.[40] The

distance of 4.0 Å is too long for sufficient ET to be induced.
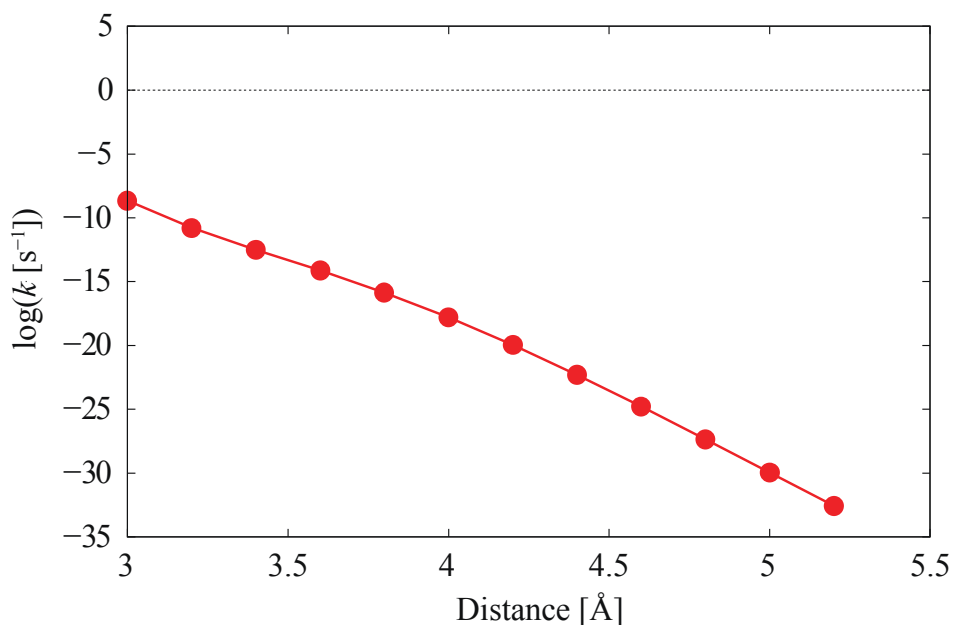

Fig. 6   Variation of the logarithm of the charge recombination factor with the

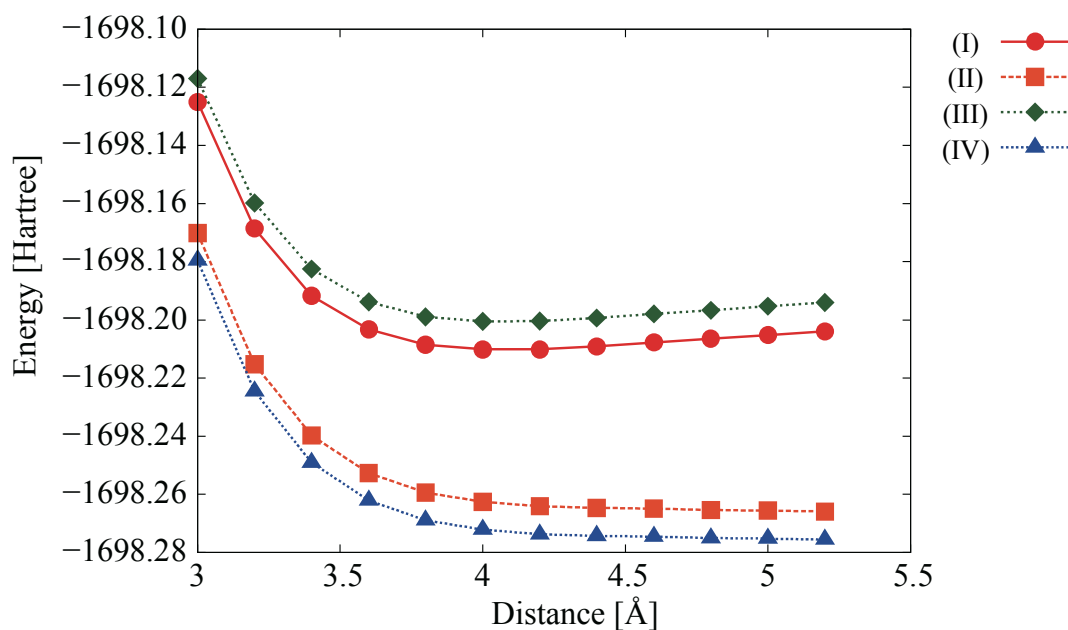**center-to-center distance of the OPV3 dimer in the face-to-face orientation.**

Fig. 7   **Energy variations of the four states (I)-(IV) with the center-to-center distance of the OPV3 dimer in the face-to-face orientation. The minima of the polaron states (I) and (III) occur at 4 Å.**

4.2   Effect of roll angle

Before giving the results for roll-rotated orientations, we give the result for

OPV3-methyl in the crystal structure to clarify the dimer orientations that are suitable

for ET. The crystal-structure orientations and the symbols representing them, T1, T2,

and P, are shown in Fig. 8. For each orientation in the OPV3-methyl crystal, the charge

recombination factors and Marcus parameters obtained from the CDFT calculations are
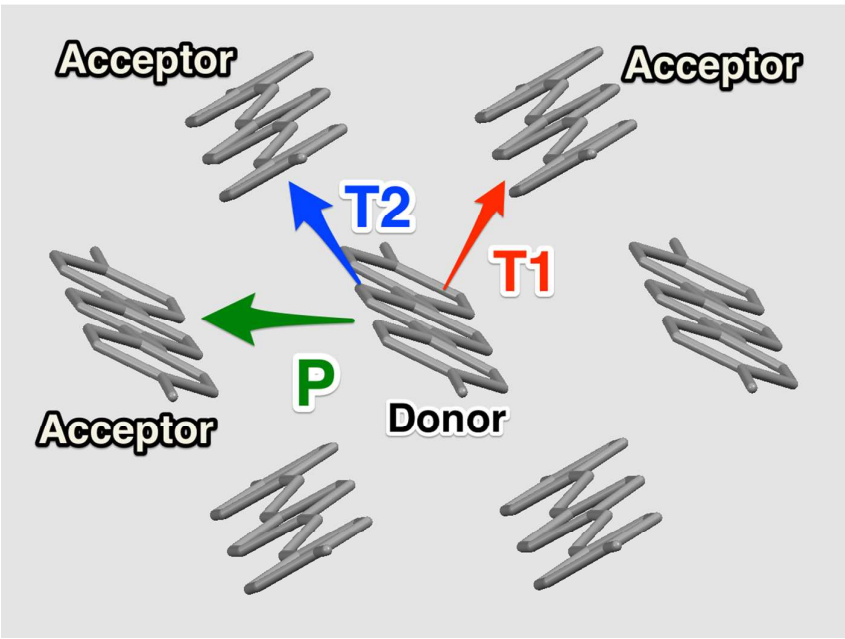
shown in Table 4.

Fig. 8   Crystal structure of OPV3-methyl. The symbols T1, T2, and P indicate the orientations of the ET channel.

Table 4   Calculated ET parameters[a] and decadic logarithm of charge recombination factor for the orientations (Fig. 8) in the crystal structure of OPV3-methyl.

Orientation	$-\Delta G^\circ$	λ	$\Delta G^\ddagger$	$|H_{ab}|$	$\log_{10}(\square \ [s^{-1}])$
T1-dimer	81.74	24.05	34.60	25.03	9.294
T2-dimer	331.4	26.08	893.6	11.20	~0 (−141.9)
P-dimer	180.4	25.86	230.7	5.266	~0 (−26.43)

[a] All energies are in kJ mol^{-1}.

Table 4 shows that the values of the recombination factor are considerably different among the orientations. In particular, the largest change among the parameters is the driving force $-\Delta G°$. Interestingly, the recombination factor of the T1-dimer is at least 10^{10} times larger than that of the T2-dimer, although in these orientations the donor and acceptor positions are reversed each other.

We investigated the results for OPV3 from various viewpoints on the basis of the results for OPV3-methyl crystal. We considered the roll rotation of either the donor or acceptor molecule, since the dimer orientations in the OPV3-methyl crystal correspond to the roll rotation by the Euler angle. Table 5 shows the charge recombination factors and the parameters for various rotation angles, and Fig. 9 shows the variation of the charge recombination factor (on a logarithmic scale) with the rotation angle on the donor and acceptor sides. For the acceptor rotation, the charge recombination factor becomes at least $10^7 (= 10^7 \text{ s}^{-1}/10^0 \text{ s}^{-1})$ times larger as the rotation angle increases from 0° to 90°, while for the donor rotation it becomes much smaller with increasing rotation angle. These results indicate that the large tilting of the acceptor causes the recombination factor to increase, and that the tilting of the donor makes the

22

recombination factor decrease to nearly zero.

Figure 10 shows the energy variations of states (I)-(IV) with the rotation angle of

each side. The energy curves of (II) and (IV) are almost the same for the acceptor and

donor rotations, while those of (I) and (III) are considerably different for the acceptor

and donor rotations. For the acceptor rotation, the energies of (I) and (III) decrease with

increasing angle. In contrast, the (I) and (III) energies increase with increasing angle of

donor rotation.

From the energy variations shown in Fig. 10, the significant angle exceeds 15˚

because for an angle of less than 15˚ the donor-acceptor distance is too short and the

system becomes unstable in all the states. In the final states (II) and (IV) with the

exciton-pair electronic structure $\{^1D\ldots^3A^*\}$, the two energy curves nearly overlap for

the donor and acceptor rotations. On the other hand, the energies of the initial states (I)

and (III) with the polaron-pair electronic structure $\{^2D^{\bullet-}\ldots^2A^{\bullet+}\}$ become more stable

with increasing angle of acceptor rotation but less stable with increasing angle of donor

rotation. It is interesting that the energy variations of (I) and (III) are considerably

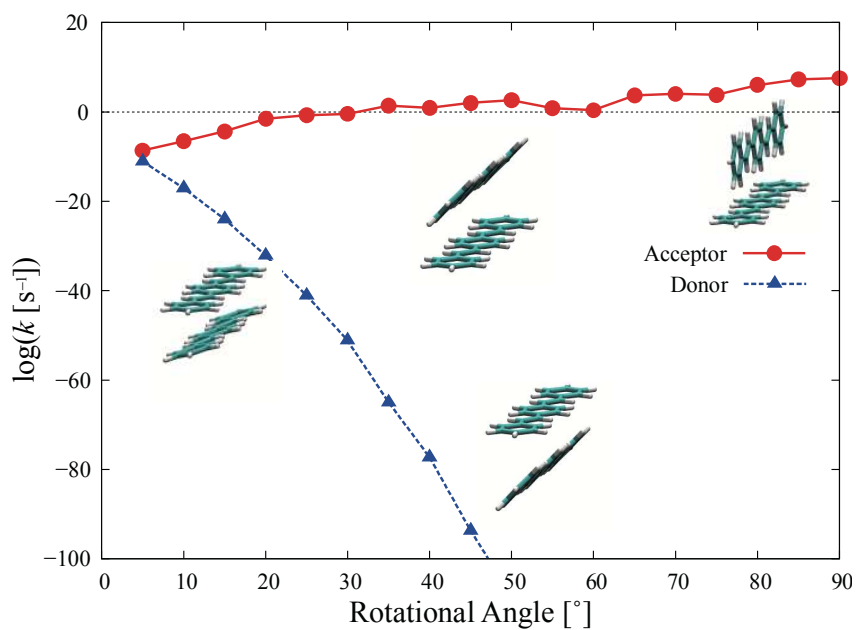different for the acceptor rotation and donor rotation.

Fig. 9 Variation of the logarithm of charge recombination factor with the roll angle of the

tilted acceptor (red filled circles) and the tilted donor (blue filled triangles) in the OPV3 dimer.
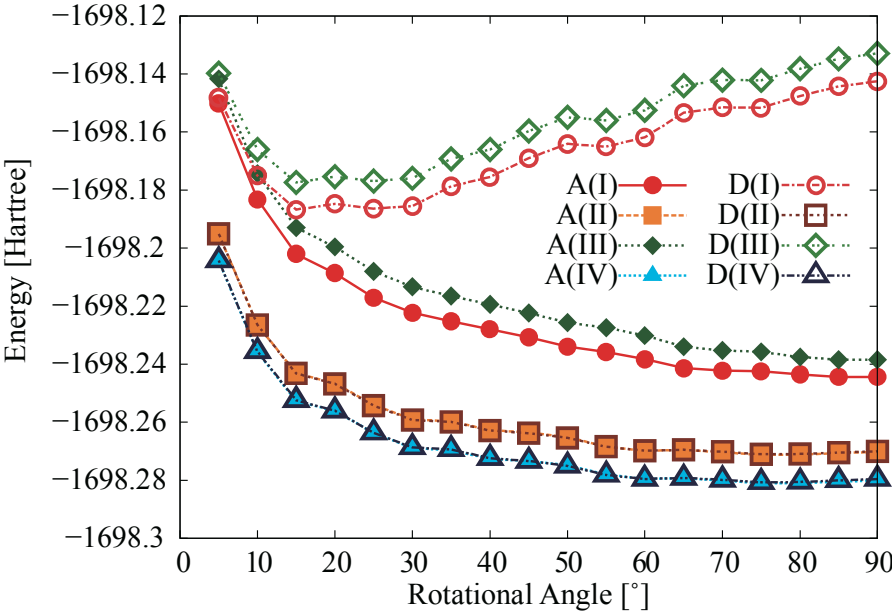
Fig. 10 **Energy variations of the four states of the OPV3 dimer with the roll angle on the acceptor side (filled symbols, A(I)-A(IV)) and donor side (open symbols, D(I)-D(IV)). The final states (II) and (IV) nearly overlap for the acceptor and donor rotations.**

Table 5 Calculated parameters[a] and decadic logarithm of charge recombination factor at various roll angles of acceptor (in the upper part) and of donor (in the lower part).

degrees [°]	$\log_{10}(\Box \ [s^{-1}])$	$-\Delta G°$	λ	$\Delta G^{\ddagger}$	$|H_{ab}|$
		acceptor rotation			
15	~0 (–4.32)	133.28	25.33	114.99	43.55
30	–0.47	122.49	25.94	89.84	23.05
45	2.04	111.99	25.85	71.74	10.82
60	0.43	108.47	25.47	67.63	0.73
75	3.82	101.40	25.75	55.56	3.20
90	7.60	93.82	25.98	44.28	25.71
		donor rotation			
15	~0 (–24.02)	172.51	24.18	227.46	43.28
30	~0 (–51.14)	218.46	24.81	377.90	18.16
45	~0 (–93.69)	273.94	25.15	615.39	6.11
60	~0 (–126.52)	309.21	25.55	787.20	0.26
75	~0 (–156.96)	338.97	25.34	970.39	1.78
90	~0 (–182.57)	359.94	25.10	1116.82	1.87

[a] All energies are in kJ mol^{-1}.

26

To explain this behavior of the energy curves in Fig. 10, the following two reasons are

considered. (i) The donor with the rich π-electron density does not face the acceptor

plane when the donor molecule rotates. For the rotation of the acceptor molecule, in

contrast, the electron-deficient side of the acceptor faces the donor with the rich

π-electron density. From this, the rotation of the acceptor is favorable for ET. (ii) The

face-to-face orientation (for a rotation of less than 15˚ in Fig. 10) forms a π-π stacking

structure, which can have a large transfer integral; however, the donor and acceptor

cannot be close owing to the electron repulsion. The energetic barrier is

disadvantageous for ET.

4.3   Effect of intermolecular distance in edge-to-face conformation

To verify the tendency discussed above, we computed the charge recombination factor

of the OPV3 dimer fixed at a rotation angle of 45˚ and varied the intermolecular

distance, i.e., the closest atomic distance between the donor and acceptor.

The difference in the charge recombination factor between the rotated donor and

rotated acceptor is clearly shown in Fig. 11. The charge recombination factor for the

acceptor rotation becomes at least 10^6 (= 10^6 s^{-1}/10^0 s^{-1}) times larger as the

intermolecular distance decreases from 3.5 to 2.7 Å, which can be seen from the

comparison of log k values at 3.5 and 2.7 Å in the upper part of Table 6. Furthermore,

we can also see that the large variation of log k from 3.5 to 2.7 Å is caused by the

variation of the driving force $-\Delta G°$, which decreases from 148.7 to 97.0 kJ/mol^{-1}. On

the other hand, the charge recombination factor for the donor rotation becomes 10^{46} (=

10^{-69} s^{-1}/10^{-105} s^{-1}) times smaller with the same change in the intermolecular distance,

which can be also checked from log k values in the lower part of Table 6. As the

intermolecular decreases, the charge recombination factor increases in the tilted

acceptor but decreases in the tilted donor.

From the energies of (I)-(IV) shown in Fig. 12, the energies of (II) and (IV) are

similar for the two cases, whereas the energies of (I) and (III) are considerably different.

An intermolecular distance of more than 2.7 Å is significant since all the states are

unstable when the distance is less than 2.7 Å. Thus, we discuss the recombination

factors only for the case that the intermolecular distance is greater than 2.7 Å. Figure 12

shows that the energies of the exciton-pair electron states $\{^1D...^3A^*\}$, (II) and (IV), have

no significant difference between the cases of acceptor and donor rotation, whereas a

large energy difference between the two cases can be seen for the polaron-pair electron

states $\{^2D^{\bullet-}...^2A^{\bullet+}\}$, (I) and (III). The rotation of the acceptor stabilizes the dimer energy,

while that of the donor destabilizes the dimer energy. Generally an anion-cation pair

becomes stable as the anion and cation approach each other. However, the approach of

the tilted donor with a negative charge (-1) to the positively charged (+1) acceptor

causes destabilization. This result confirms that the rotated acceptor can easily approach

the donor to within a distance of ~2.7 Å, whereas the rotated donor cannot approach

close to the acceptor.

Finally, in the present study, we have not accounted for the dispersion effect, which is

important in the intermolecular interaction of the present π-systems.   Since the B3LYP

functional and 6-31G(d) basis set used in the present calculations does not suitably

evaluate such dispersion effects, we tried to add Grimme's dispersion correction[41] with

the present CDFT energies. For Table 5, we reexamined the CDFT result including the

dispersion correction, which is given in Table 5S of the supporting information, and

found that the dispersion effect in the recombination factor is rather minor at the present

computational level. However, the Grimme's dispersion correction is not sufficiently

worked with middle-size basis sets such as 6-31G(d), and we need larger basis set added

with the advanced dispersion correction such as DFT-D2[42] or DFT-D3[43,44] to evaluate

the intermolecular interaction correctly, which we remain as our future works.
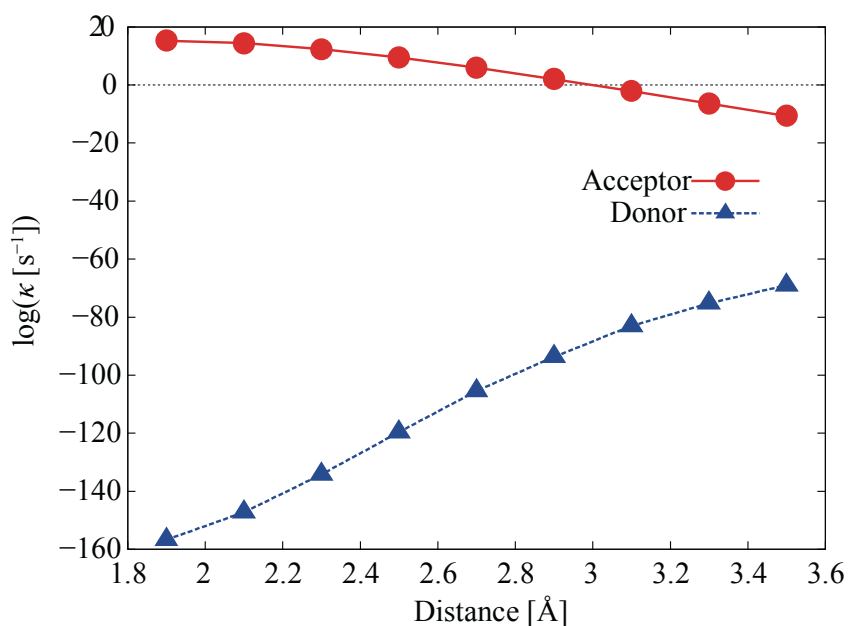
30

Fig. 11   **Variation of logarithmic of the charge recombination factor with the**

intermolecular distance, i.e., the closest atomic distance between the donor and acceptor in the

OPV3 dimer, where the rotational angle of the acceptor (red filled circles) or the donor (blue

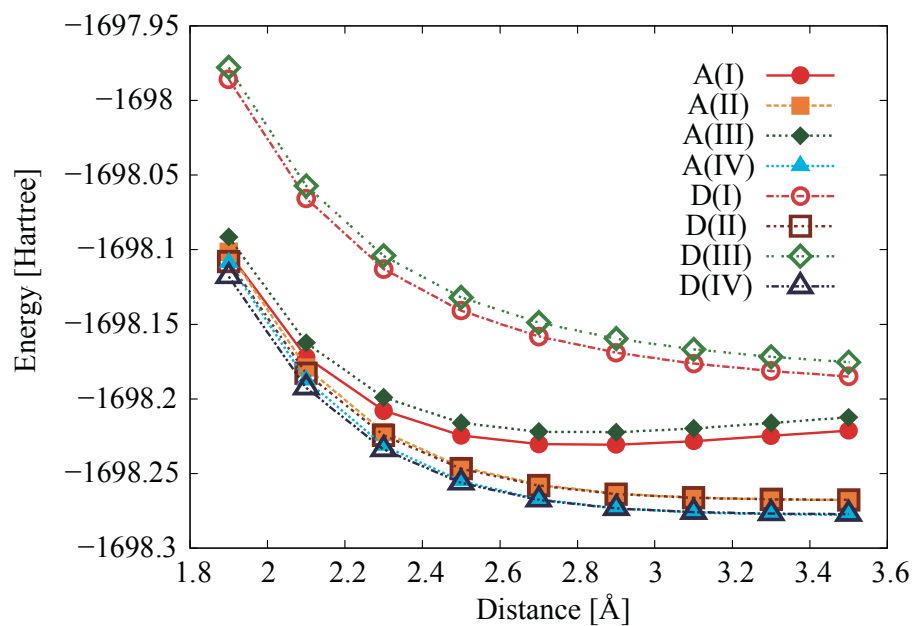**filled triangles) is fixed at 45° and the intermolecular distance is varied.**

Fig. 12   **Energy variations of (I)-(IV) states of OPV3 dimer with the intermolecular distance.**

Two cases are described in the same way as in Fig. 11; the rotational angle on the acceptor side

(filled symbols, A(I)-A(IV)) or the donor side (open symbols, D(I)-D(IV)) is fixed at 45°. The

minima of A(I) and A(III) occur at 2.7 Å.

Table 6 Calculated charge recombination parameters[a] and decadic logarithm of charge recombination factor for various closest-contact distances of acceptor at 45° (in the upper part) and donor at 45° (in the lower part) in the OPV3 dimer.

distance [Å]	$\log_{10}(\square\ [s^{-1}])$	$-\Delta G°$	λ	$\Delta G^{\ddagger}$	$|H_{ab}|$
acceptor rotation					
1.9	15.29	17.98	19.54	0.03	22.31
2.3	12.35	61.44	23.89	14.75	15.40
2.7	5.95	97.00	25.55	49.97	11.94
3.1	–2.13	125.64	26.06	95.11	9.92
3.5	~ 0 (–10.66)	148.71	26.21	143.10	8.65
donor rotation					
1.9	~ 0 (–156.74)	347.36	26.20	984.03	36.12
2.3	~0 (–134.27)	317.89	25.14	852.42	18.11
2.7	~0 (–105.48)	287.79	25.18	684.57	8.90
3.1	~ 0 (–83.07)	261.54	25.25	552.79	4.12
3.5	~ 0 (–69.02)	242.44	25.19	468.35	1.74

[a] All energies are in kJ mol^{-1}.

5. Conclusions

In the present work, we have investigated the intermolecular triplet-triplet ET of the

OPV3 dimer as a model system for the PPV charge recombination process by using

CDFT. In addition, we analyzed the relation between the intermolecular orientation of

the dimer and the recombination factor to provide guidelines for molecular design of

effective charge recombination systems. It was found that the face-to-face orientation

has a low recombination factor of 10^{-18} s^{-1} at an intermolecular distance of 4.0 Å, where

the polaron states (I) and (III) have energy minima. The value of 10^{-18} s^{-1} for the

face-to-face orientation is much lower than that of 10^6 s^{-1} for the edge-to-face

orientation at the intermolecular distance of 2.7 Å with 45˚ rotation of the acceptor.

In the edge-to-face case, the roll rotation of the donor molecule causes the charge

recombination factor to decrease to nearly zero, whereas that of the acceptor molecule

increases the recombination factor to the order of 10 s^{-1}. Regarding the energies of the

four states, those of the final exciton-pair states (II) and (IV) are almost the same for

both donor rotation and acceptor rotation, whereas for the initial polaron-pair states (I)

and (III), the energies of the acceptor rotation become much lower than those of the

donor rotation with increasing angle of rotation. This induces a large difference in the

driving force $-\Delta G°$ between the two cases, which ultimately causes the difference in the

recombination factors.

We carried out the calculation for the dimer with several intermolecular distances and

a fixed rotation angle (45°) to investigate how the difference between the tilted

molecules occurs. The approach of the tilted donor to the flat acceptor decreases the

recombination factor, while the approach of the tilted acceptor to the flat donor

increases the recombination factor. The polaron states become stable in the former case

(at least down to an intermolecular distance of 2.7 Å), while they become unstable in

the latter case. From the results, we can conclude that the flat-donor and tilted-acceptor

pair is a more favorable orientation for triplet-triplet charge recombination than the

tilted-donor and flat-acceptor pair.

The present computational results show that the molecular orientation is a very

important factor for material design, and suggests that single crystals with a herringbone

structure such as rubrene and tetracene have higher hole-mobility than those with a

lamella structure with large transfer integrals.

The present results would also be helpful for readers of supramolecular chemistry and

related fields. For example, orientation and organization of p-phenylenevinylene

derivatives have been paid much attention.[45] In some cases, orientation and

arrangements of the component chromophores are highly controlled and modified. It is

noted that the methyl-substituted system, OPV3-methyl, has larger value in charge

recombination factor than the non-substituted OPV3 as shown in Table 2. This suggests

a possibility that the OPV3 derivatives with various functional groups have large charge

recombination factor. Thus, the CDFT calculations for several OPV3 derivatives are

now in progress, and the substitution effect, as well as the molecular orientation effect,

on the charge recombination processes would be clear soon.

36

Acknowledgements

Appendix

Fragmented initial density matrix for CDFT calculations

To improve the convergence in the CDFT calculations, we applied the fragmented

initial density matrix comprising the monomer charge densities. For instance, in Fig. 5

the charge density matrices $\mathbf{D}_1$ of Region C and $\mathbf{D}_2$ of Region NC are put on the

diagonal blocks of the initial density matrix of the dimer as follows:

$$\mathbf{D} = \begin{pmatrix} \mathbf{D}_1 & 0 \\ 0 & \mathbf{D}_2 \end{pmatrix}.$$

Using this initial density matrix can decrease the number of required CDFT-SCF cycles

and speed up the convergence. We confirmed that the computational results agreed with

those obtained without using the fragmented initial density matrix in several test

calculations.

References

1   Y. Yamashita, *Sci. Technol. Adv. Mater.*, 2009, **10**, 024313.

2   V. Coropceanu, J. Cornil, D. A. da Silva Filho, Y. Olivier, R. Silbey and J.-L. Brédas, *Chem. Rev.*, 2007, **107**, 926–952.

3   C. Wang, H. Dong, W. Hu, Y. Liu and D. Zhu, *Chem. Rev.*, 2012, **112**, 2208–2267.

4   S. Günes, H. Neugebauer and N. S. Sariciftci, *Chem. Rev.*, 2007, **107**, 1324–1338.

5   F. C. Grozema, P. T. van Duijnen, Y. A. Berlin, M. A. Ratner and L. D. A. Siebbeles, *J. Phys. Chem. B*, 2002, **106**, 7791–7795.

6   H. Dong, X. Fu, J. Liu, Z. Wang and W. Hu, *Adv. Mater.*, 2013, **25**, 1–25.

7   S. Watanabe, Y. Shimodo and K. Morihashi, *Theor. Chem. Acc.*, 2011, **130**, 807–813.

8   L. Wang, G. Nan, X. Yang, Q. Peng, Q. Li and Z. Shuai, *Chem. Soc. Rev.*, 2010, **39**, 423–434.

9   J. Mei, Y. Diao, A. L. Appleton, L. Fang and Z. Bao, *J. Am. Chem. Soc.*, 2013, **135**, 6724–6746.

10   W. Geens, S. E. Shaheen, B. Wessling, C. J. Brabec, J. Poortmans and N. S. Sariciftci, *Org. Electron.*, 2002, **3**, 105–110.

11   A. Inigo, H.-C. Chiu, W. Fann, Y.-S. Huang, U.-S. Jeng, T.-L. Lin, C.-H. Hsu, K.-Y. Peng and S.-A. Chen, *Phys. Rev. B*, 2004, **69**, 075201.

12   E. H. A. Beckers, S. C. J. Meskers, A. P. H. J. Schenning, Z. Chen, F. Würthner, P. Marsal, D. Beljonne, J. Cornil and R. A. J. Janssen, *J. Am. Chem. Soc.*, 2006, **128**, 649–657.

13   M. D. Curtis, J. Cao and J. W. Kampf, *J. Am. Chem. Soc.*, 2004, **126**, 4318–4328.

14   M. Ottonelli, D. Duce, S. Thea and G. Dellepiane, *J. Nanosci. Nanotechnol.*, 2013, **13**, 5186–5193.

15   M. Mas-Torrent, P. Hadley, S. T. Bromley, X. Ribas, J. Tarrés, M. Mas, E. Molins, J. Veciana and C. Rovira, *J. Am. Chem. Soc.*, 2004, **126**, 8546–8553.

16   V. C. Sundar, J. Zaumseil, V. Podzorov, E. Menard, R. L. Willett, T. Someya, M. E. Gershenson and J. A. Rogers, *Science*, 2004, **303**, 1644–1646.

17   U. Sondermann, A. Kutoglu and H. Bässler, *J. Phys. Chem.*, 1985, **89**, 1735–1741.

18   R. N. Marks, J. J. Halls, D. D. C. Bradley, R. H. Friend and A. B. Homest, *J. Phys. Condens. Matter*, 1994, **6**, 1379–1394.

19   Y. Cao, I. Parker, G. Yu, C. Zhang and A. Heeger, *Nature*, 1999, **397**, 414–417.

20   Z. Shuai, D. Beljonne, R. J. Silbey and J. L. Brédas, *Phys. Rev. Lett.*, 2000, **84**, 131–134.

21   D. Beljonne, A. Ye, Z. Shuai and J.-L. Brédas, *Adv. Funct. Mater.*, 2004, **14**, 684–692.

22   J.-L. Brédas, D. Beljonne, V. Coropceanu and J. Cornil, *Chem. Rev.*, 2004, **104**, 4971–5004.

23   T. Granier, E. L. Thomas, D. R. Gagnon, F. E. Karasz and R. W. Lenz, *J. Polym. Sci. B*, 1986, **24**, 2793–2804.

24   U. Jeng, C.-H. Hsu, H.-S. Sheu, H.-Y. Lee, A. R. Inigo, H. C. Chiu, W. S. Fann, S. H. Chen, A. C. Su, T.-L. Lin, K. Y. Peng and S. A. Chen, *Macromolecules*, 2005, **38**, 6566–6574.

25   Q. Wu and T. Van Voorhis, *Phys. Rev. A*, 2005, **72**, 024502.

26   Q. Wu and T. Van Voorhis, *J. Chem. Phys.*, 2006, **125**, 164105.

27   Q. Wu and T. Van Voorhis, *J. Chem. Theory Comput.*, 2006, **2**, 765–774.

28   Q. Wu and T. Van Voorhis, *J. Phys. Chem. A*, 2006, **110**, 9212–9218.

29   B. Kaduk, T. Kowalczyk and T. Van Voorhis, *Chem. Rev.*, 2012, **112**, 321–370.

30   The X-ray structural data of the OPV3-methyl single crystal was supplied by Idemitsu Kosan Co. Ltd.

31   R. A. Marcus, *J. Chem. Phys.*, 1956, **24**, 966.

32   E. Deiss, A. Wokaun, J.-L. Barras, C. Daul and P. Dufek, *J. Electrochem. Soc.*, 1997, **144**, 3877–3881.

33   M. Lundberg and P. E. M. Siegbahn, *J. Chem. Phys.*, 2005, **122**, 224103.

34   J. Perdew and A. Zunger, *Phys. Rev. B*, 1981, **23**, 5048–5079.

35   V. Anisimov, J. Zaanen and O. Andersen, *Phys. Rev. B*, 1991, **44**, 943–954.

36   H. Iikura, T. Tsuneda, T. Yanai and K. Hirao, *J. Chem. Phys.*, 2001, **115**, 3540.

37   Q. Wu, C.-L. Cheng and T. Van Voorhis, *J. Chem. Phys.*, 2007, **127**, 164119.

38   M. J. Frisch, G. W. Trucks, H. B. Schlegel, G. E. Scuseria, M. A. Robb, J. R. Cheeseman, G. Scalmani, V. Barone, B. Mennucci, G. A. Petersson, H. Nakatsuji, M. Caricato, X. Li, H. P. Hratchian, A. F. Izmaylov, J. Bloino, G. Zheng, J. L. Sonnenberg, M. Hada, M. Ehara, K. Toyota, R. Fukuda, J. Hasegawa, M. Ishida, T. Nakajima, Y. Honda, O. Kitao, H. Nakai, T. Vreven, J. A. Montgomery, Jr., J.

E. Peralta, F. Ogliaro, M. Bearpark, J. J. Heyd, E. Brothers, K. N. Kudin, V. N. Staroverov, R. Kobayashi, J. Normand, K. Raghavachari, A. Rendell, J. C. Burant, S. S. Iyengar, J. Tomasi, M. Cossi, N. Rega, N. J. Millam, M. Klene, J. E. Knox, J. B. Cross, V. Bakken, C. Adamo, J. Jaramillo, R. Gomperts, R. E. Stratmann, O. Yazyev, A. J. Austin, R. Cammi, C. Pomelli, J. W. Ochterski, R. L. Martin, K. Morokuma, V. G. Zakrzewski, G. A. Voth, P. Salvador, J. J. Dannenberg, S. Dapprich, A. D. Daniels, Ö. Farkas, J. B. Foresman, J. V. Ortiz, J. Cioslowski and D. J. Fox, 2009.

39   T. Ogawa, M. Sumita, Y. Shimodo and K. Morihashi, *Chem. Phys. Lett.*, 2011, **511**, 219–223.

40   C. R. Martinez and B. L. Iverson, *Chem. Sci.*, 2012, **3**, 2191–2201.

41   S. Grimme, *J. Comput. Chem.*, 2004, 25, 1463-1473.

42   S. Grimme, *J. Comput. Chem.*, 2006, 27, 1787-1799.

43   S. Grimme, J. Antoney, S. Ehrlich and H. Krieg, *J. Chem. Phys.*, 2010, 132, 154104.

44   S. Grimme, S. Ehrlich and L. Goerigk, *J. Comput. Chem.*, 2011, 32, 1456-1465.

45   K. Sakakibara, P Chithra, B. Das, T. Mori, M. Akada, J. Labuta, T. Tsuruoka, S. Maji, S. Furumi, L. K. Shrestha, J. P. Hill, S. Acharya, K. Ariga and A. Ajayaghosh, *J. Am. Chem. Soc.*, 2014, 136, 8548-8551.